J. Fluid Mech. (2006), *vol.* 565, *pp.* 227–253.
doi:10.1017/S0022112006001601 Printed in the United Kingdom

Axisymmetric gravity currents on a cone

By ANDREW N. ROSS[1], STUART B. DALZIEL[2] AND P. F. LINDEN[3]

[1]Institute for Atmospheric Science, School of Earth and Environment, University of Leeds, Leeds, LS2 9JT, UK

[2]Department of Applied Mathematics and Theoretical Physics, Centre for Mathematical Sciences, University of Cambridge, Wilberforce Road, Cambridge, CB3 0WA, UK

[3]Department of Mechanical and Aerospace Engineering, University of California, San Diego, 9500 Gilman Drive, La Jolla, CA 92093-0411, USA

aross@env.leeds.ac.uk

(Received 25 January 2004 and in revised form 15 March 2006)

The previously unstudied problem of an axisymmetric gravity current released on a cone is investigated. A formulation of the problem based on the shallow-water equations, with and without entrainment and bottom drag, is given. Analytical asymptotic solutions are found and compared to numerical solutions of the equations. The inclusion of entrainment and drag is seen to play a significant role in limiting the propagation speed of the gravity current and also in altering the shape of the current. These theoretical predictions are compared to laboratory experiments and to two-dimensional numerical simulations. The shallow-water solutions including entrainment are found to provide a much better comparison with the experiments than the solutions without entrainment. In particular, the observed front speed and dilution of the head are in good agreement. Some applications to industrial and environmental problems such as dense gas dispersion are briefly discussed.

1. Introduction

There are many industrial, geophysical and environmental situations in which a fluid spreads into a lighter (or denser) fluid as a result of the density difference. One major example of relevance to industry is the spread of a dense gas following a chemical spillage. Many poisonous, corrosive, explosive or suffocating gases are routinely manufactured or used in the chemical industry and these gases are often denser than air. The consequences of a spillage of such a gas can be disastrous, as illustrated by the terrible accident at Bhopal, India, in 1984 in which thousands of people died. In order to assess the risk in the event of an accident it is necessary to understand the dynamics of the dense gas cloud. The related problem of a light gas is equally important; for instance the release of methane (which is lighter than air) in a mine tunnel can result in the methane flowing along the roof of the tunnel.

Flows such as these, which are driven by horizontal density gradients, are known as gravity currents. While much research has been done into these flows, the majority of it has concentrated on gravity currents flowing along a horizontal boundary. Attention has also been focused on either channel flows or axisymmetric flows. These two-dimensional cases are much simpler to model theoretically and to study in the laboratory. Simpson (1997) provides a good overview of the literature.

Previous studies have looked at gravity currents in a sloping channel (Britter & Linden 1980; Beghin, Hopfinger & Britter 1981; Cheong & Han 1997; Webber, Jones & Martin 1993; Montgomery & Moodie 1999), but there are few industrial situations which can realistically be modelled as such. Some studies (e.g. Webber *et al.* 1993; Tickle 1996; Ross, Linden & Dalziel 2002) have also considered an instantaneous release on an inclined plane. The problem of a gravity current on a cone has been neglected, but may be much more relevant. Chemical or industrial facilities storing dense gases may be situated on the top of a hill or in the bottom of a valley. In this case it may be appropriate to consider the geometry as axisymmetric rather than as channel flow or a uniform slope. In many chemical plants the facilities are placed on a mound of earth surrounded by circular containment bunds, again giving rise to an axisymmetric sloping geometry. The instantaneous release of a gravity current on a cone provides an idealization of these problems. The flow need not be over the whole of the cone. For instance, a valley may become wider with distance down the mountain, and a sector of a cone would provide a good model for the flow in such a valley. There will of course be some difference in curvature on the slope since a valley floor would tend to be concave in the across-valley direction, while a sector of a cone will have convex curvature in this direction. However, this curvature will be a relatively small correction in many circumstances when compared to the slope and the divergence of the valley. This paper will concentrate on problems involving the instantaneous release of a fixed volume of dense fluid.

In § 2 a shallow-water model for a gravity current on a cone, including the effects of entrainment and drag, is presented. Asymptotic behaviour is examined, both with and without entrainment and drag, and compared with numerical solutions. In § 3 a two-dimensional numerical model for studying gravity currents is described. Section 4 describes laboratory experiments to measure saline gravity currents in a tilted sector tank. These laboratory experiments are compared to the theoretical and numerical models in § 5. Final conclusions are given in § 6.

2. A shallow-water model for flow down a cone

2.1. *Model equations*

The shallow-water equations have been extensively used to model gravity currents on a flat surface (e.g. Grundy & Rottman 1985; Bonnecaze, Huppert & Lister 1993) with both similarity solutions and numerical solutions being available for a variety of problems. Provided the slope angle is not too large, the shallow-water equations can also be used to describe the flow of a gravity current on a slope. More formally we require that the slope angle, θ, satisfies $\tan\theta \ll 1$, which is consistent with the shallow water approximation that the horizontal scale of changes in the flow is much larger than the vertical scale. Webber *et al.* (1993) and Tickle (1996) used this approach to model a gravity current in a sloping channel or on a uniform slope. The model of Webber *et al.* (1993) neglected the effect of entrainment, but subsequent studies by Tickle (1996) and Ross *et al.* (2002) have shown that entrainment can play an important role in controlling a gravity current on a slope. The shallow-water similarity solutions of Webber *et al.* (1993) tend to overpredict the propagation speed as a result of neglecting entrainment.

In this paper the shallow-water equations will be used to model a different sloping geometry with an axisymmetric gravity current being released on the top of a cone. The flow is assumed to be Boussinesq so that density variations are neglected, except in the buoyancy term where they appear combined with gravity. Under this

Variable	Non-dimensionalize w.r.t.
h, r	$V^{1/3}$
t	$V^{1/6}g_0'^{-1/2}$
u	$V^{1/6}g_0'^{1/2}$
g'	g_0'

TABLE 1. Details of the non-dimensionalization of the shallow-water equations.

assumption the effective gravity is defined as $g' = g(\rho - \rho_0)/\rho_0$ where ρ is the density of the current and ρ_0 is the background density. Here an entrainment term (based on the entrainment assumption of Morton, Taylor & Turner 1956) is included in the shallow-water equations, so the rate at which fluid is entrained through the interface on the top of the gravity current is proportional to the speed of the flow. The empirical constant of proportionality, α, is know as the entrainment coefficient and determines the amount of ambient fluid entrained into the current. Also included is a bottom drag term which is proportional to the speed squared and acts to oppose the flow. The constant of proportionality is the drag coefficient, C_d. In polar coordinates the non-dimensional axisymmetric shallow-water equations for mass, momentum and effective gravity are

$$\frac{\partial h}{\partial t} + \frac{1}{r}\frac{\partial (ruh)}{\partial r} = \alpha |u|, \tag{2.1}$$

$$\frac{\partial}{\partial t}(uh) + \frac{1}{r}\frac{\partial}{\partial r}(ru^2 h) + \frac{\partial}{\partial r}\left(\frac{1}{2}g'h^2\right) - g'h\tan\theta = -C_d u^2, \tag{2.2}$$

and

$$\frac{\partial}{\partial t}(g'h) + \frac{1}{r}\frac{\partial}{\partial r}(rug'h) = 0, \tag{2.3}$$

where h is the vertical height of the fluid layer above the cone, u is the speed of the flow and r is the horizontal distance from the origin of the cone.

The front boundary condition is that

$$F = \frac{u_f}{(g_f' h_f)^{1/2}}, \tag{2.4}$$

where the subscript f denotes the value of the variable at the front of the gravity current and F is the (prescribed) Froude number.

The equations are non-dimensionalized with respect to the lengthscale $V^{1/3}$ and the timescale $V^{1/6}/g_0'^{1/2}$ as shown in table 1. The non-dimensionalization depends only on V and g_0', which characterize the size and density of the gravity current, and not on the details of the initial release itself. This is particularly useful when seeking long-time asymptotic solutions which are not expected to depend on the details of the initial release. From now on all variables are non-dimensional unless otherwise stated. The Froude number condition, (2.4), remains unchanged by the non-dimensionalization.

Various laboratory experiments (see e.g. Huppert & Simpson 1980) have shown that for gravity currents where the head occupies a small fraction of the total depth of the fluid the Froude number has a constant value of about 1.19. Huppert & Simpson (1980) also investigated the initial stages of a gravity current release where the fractional depth was not small. For fraction head depths, ϕ, greater than 0.075 they proposed the empirical relationship $F = \frac{1}{2}\phi^{-1/3}$. This relationship for F will be used for numerical solutions of the shallow-water equations. When seeking asymptotic

solutions the assumption is made that for long times the precise initial conditions of the release are not important in determining the flow, and only the bulk properties such as the initial buoyancy need be considered. Consistent with this we neglect the initial variation in Froude number with fractional depth and assume a constant Froude number throughout for asymptotic solutions. One further constraint on the solution is conservation of the total non-dimensional buoyancy, $\int_0^{r_f} 2\pi r g' h \, \mathrm{d}r = 1$, where r_f is the position of the front of the gravity current.

In this formulation of the shallow-water equations viscosity is neglected. For high-Reynolds-number flows this is a reasonable assumption. There is no explicit modelling of the turbulence in the equations; however the effects of turbulence are implicitly included through the Froude number condition at the front and through the entrainment and bottom drag. The values of the constants in these parameterizations are determined empirically from experiments.

A typical value for α from experiments of entrainment into a plume (see e.g. Morton *et al.* 1956) would be 0.1. In studying entrainment into a layer of stratified fluid in a sloping channel Ellison & Turner (1959) found a dependence of α on the Richardson number of the layer, $Ri = g'h/U^2$ where g' is the effective gravity of the layer, h is the depth of the layer and U is its speed. The steady-state value of Ri depended on the slope and leads to an entrainment increasing with slope. For a slope of about 10° the entrainment coefficient was approximately 0.02. The experiments of Ross *et al.* (2002) for a gravity current on a uniform inclined plane compared well with an integral model for the development of the gravity current assuming an entrainment coefficient of 0.1. In this case entrainment was assumed to be limited to a region near the head. It could be argued that near the head of a gravity current more entrainment might be expected. Since this region controls the propagation and development of the current, a larger value of α may be more appropriate in these experiments. Experiments by Hallworth *et al.* (1996) for gravity currents on a horizontal surface gave a value of 0.063 for the entrainment coefficient. In these experiments the head was observed to remain almost undiluted during the initial slumping phase, with entrainment only becoming important subsequently.

The bottom drag coefficient, C_d, is also the subject of some uncertainty. For gravity currents in a smooth sloping channel Britter & Linden (1980) found a value of about 0.003 for the drag coefficient. Ellison & Turner (1959) work on the assumption that it is less than 0.02. In either case the value is likely to be no larger than the entrainment coefficient and may well be much smaller. We shall investigate the dependence of the solution on the values taken for both α and C_d.

Flow in the layer above the gravity current is neglected in this single-layer shallow-water approximation, except through the Froude number dependence on fractional depth. This is a reasonable assumption for this problem since the ambient layer rapidly becomes much deeper than the gravity current as a result of the radial expansion of the current and the increase in depth due to the sloping bottom. However, the single-layer model will underestimate the time for the rarefraction wave generated from a lock release to be reflected from the axis and catch up with the front again (Ungarish & Zemach 2005), a problem that is compounded in the sloping case.

In §2.2 and §2.3 analytical solutions for these shallow-water equations will be derived. In particular, long-time asymptotic solutions will be sought; that is, solutions which are valid for time $t \gg 1$ such that the flow is no longer dependent on the precise details of the release, merely on the bulk initial quantities V and g'_0. This motivates the choice of non-dimensionalization above in terms of these quantities rather than of the initial dimensions of the release. It is generally assumed that for any initial

conditions the exact (possibly numerical) solution of the initial value problem will tend to the asymptotic solution as $t \to \infty$. This will be checked for several cases in § 2.4 using numerical solutions of the shallow water equations.

2.2. *Asymptotic behaviour without entrainment or drag*

In the absence of entrainment ($\alpha = 0$) the gravity current is not diluted, $g' \equiv 1$ and (2.3) reduces to (2.1). Assuming also that there is no bottom drag ($C_d = 0$), the resulting pair of equations can be written as

$$\frac{\partial h}{\partial t} + \frac{1}{r}\frac{\partial (ruh)}{\partial r} = 0 \tag{2.5}$$

and

$$\frac{\partial u}{\partial t} + u\frac{\partial u}{\partial r} + \frac{\partial h}{\partial r} - \tan\theta = 0, \tag{2.6}$$

with $F = u_f/\sqrt{h_f}$ at the front of the current. Global conservation of volume in the current gives $2\pi \int_0^{r_f} rh \, \mathrm{d}r = 1$.

At large radii the current will have spread such that the front speed is small and only relatively slowly varying. The dominant $\tan\theta$ term in (2.6) must therefore be principally balanced by the $\partial h/\partial r$ term. This implies that the top of the current is almost horizontal, as with the similarity solution of Webber *et al.* (1993) for a gravity current on an inclined plane. In this case the balance is not exact however. Suppose then that the gravity current takes the form of a ring with front height h_f and front position r_f travelling with a uniform speed. The top of the current is horizontal and has length l so $h_f = l\tan\theta$. Global conservation of volume gives $l = (r_f \pi \tan\theta)^{-1/2}$. Using the Froude number condition at the front of the current requires $u = u_f = F\,(\tan\theta/(\pi r_f))^{1/4}$. Integrating this gives $r_f = (\tan\theta/\pi)^{1/5}(5F\,t/4)^{4/5}$. These expressions for u and h provide a leading-order solution (in powers of $r_f^{-1/4}$) to (2.5) and (2.6) for $r_f \tan\theta \gg 1$. The neglected terms in the expansions for u and h are $O(r_f^{-3/2})$ or smaller. An expansion for u and h to the next order is given in Appendix A.

Note that as the slope becomes small the $\tan\theta$ term in (2.6) becomes smaller, and so it takes a longer time from the release until this becomes the dominant term. As $\theta \to 0$ this solution will never be reached. There is, however, an exact similarity solution to (2.1)–(2.3) with $\theta = 0^\circ$ and $\alpha = 0$ with $r_f \propto t^{1/2}$ (see Grundy & Rottman 1985; Bonnecaze *et al.* 1995, for details).

2.3. *Asymptotic behaviour with entrainment and drag*

Comparison of terms in (2.1)–(2.3) suggests rewriting the problem in terms of $\eta = r/r_f$ and t, where r_f is the position of the gravity current front. This ensures the current lies in the region $0 \leqslant \eta \leqslant 1$. In order to seek a similarity solution, we write

$$u = rt^{-1}U(\eta), \quad h = rH(\eta), \quad g' = rt^{-2}G(\eta). \tag{2.7 a–c}$$

These expressions can be substituted into (2.1)–(2.3). The front Froude number condition $u_f = F\sqrt{g'_f h_f}$, the condition $u_f = \dot{r}_f$ and the requirement that the total buoyancy of the current is conserved ($\int_0^{r_f} 2\pi r g' h \, \mathrm{d}r = 1$) allow the ensuing system of ordinary differential equations for U, H and G to be solved. One further condition, that h remains finite at $r = 0$, is also assumed. This gives the similarity solution

$$r_f = t^{1/2}\left[\frac{2\pi}{A}\left(-\frac{1}{4}\left(1 + \frac{3C_d}{2\alpha}\right) + \left(\frac{A}{4F^2} + 1 + \frac{3C_d}{2\alpha}\right)\frac{1}{4 - A}\right)\right]^{-1/4}, \tag{2.8a}$$

$$U(\eta) = \tfrac{1}{2}, \tag{2.8b}$$

$$H(\eta) = \tfrac{1}{3}\alpha, \tag{2.8c}$$

$$G(\eta) = \frac{3}{\alpha}A^{-1}\left(-\left(1+\frac{3C_d}{2\alpha}\right)+\left(\frac{A}{4F^2}+1+\frac{3C_d}{2\alpha}\right)\eta^{-A}\right), \tag{2.8d}$$

where

$$A = 3 - \frac{6\tan\theta}{\alpha}. \tag{2.9}$$

The introduction of entrainment gives rise to a very different form for the gravity current. Without entrainment the asymptotic solution is, to leading order, one in which the majority of the dense fluid remains in a relatively small region (with width and height scaling on $r_f^{1/2}$) near the head of the gravity current. This head propagates down the slope. In contrast, the similarity solution given by (2.8) has a finite depth along the entire length of the slope for all times. The entrainment prevents the current from being divided into a head region and a much thinner tail. As a result of the dilution of the head, the front speed is reduced slightly compared to the non-entraining case and is proportional to $t^{1/2}$ rather than $t^{4/5}$. It is interesting to note that this similarity solution predicts that the depth of fluid at a point remains constant, with the increase due to entrainment being balanced by the advection of fluid down the slope.

This solution is not universally valid however. From (2.7) and (2.8) it can be seen that $g' \propto \eta t^{-3/2} G(\eta)$, which contains a term proportional to $\eta^{(1-A)}$. For $A > 1$, this term will become infinite as $\eta \to 0$ (i.e. near the origin) at all times, which is clearly physically unreasonable. For $A < 1$, the solution for g' remains finite for $0 \leqslant \eta \leqslant 1$ for all times. For a given η we see $g' \propto t^{-3/2}$ and so for large times g' will not only be finite, but will be smaller than the initial effective gravity, g'_0. This condition on A translates to the requirement that

$$\tan\theta \geqslant \alpha/3, \tag{2.10}$$

i.e. in order for the similarity solution to be physically realistic the slope must be sufficiently large to meet this inequality. For a typical value of $\alpha = 0.1$ this gives a minimum slope of about 1.9°, with correspondingly smaller slopes for smaller values of α. The condition (2.10) on the slope and entrainment must be satisfied, irrespective of the drag. Provided it is satisfied, then the addition of drag imposes no extra constraint on the validity of the solution. Like the entrainment, the drag acts to slow down the propagation of the gravity current. It differs from the entrainment in that it only alters the dilution of the current indirectly through changing the speed of the current. By considering just the propagation speed of a gravity current it is impossible to derive from this solution the relative importance of entrainment and drag. This can only be done by also comparing the asymptotic solution with measured profiles of height or density. The requirement that the shallow-water approximation is valid ($\tan\theta \ll 1$) puts an upper limit on the slope for which these asymptotic solutions can be applied. For a slope with $\theta = 10°$ then $\tan\theta = 0.176$, so realistically the solutions cannot strictly be applied to much larger slopes. This gives a relatively small, but practically important, range of slopes over which these asymptotic solutions are useful.

It is interesting to note that this solution with entrainment and drag has the same functional form for the speed of the current and the front position as the non-entraining solution in the absence of a slope with $r_f \propto t^{1/2}$. Comparing (2.8)

with the solution of Bonnecaze *et al.* (1995) shows that the coefficient in front of the expression for r_f is slightly different between the two cases.

An analogous solution to the shallow-water equations with entrainment and drag exists for a gravity current in a sloping channel. Details are given in Appendix B. Comparison of this to the non-entraining solution in a sloping channel given by Webber *et al.* (1993) shows that the entrainment and drag again act to limit the acceleration down the slope due to gravity.

2.4. *Numerical solutions*

In order to obtain full numerical solutions to the shallow-water equations, (2.1) and (2.2) were written in terms of $\eta = r/r_f$ and t. This ensures that the current always lies in the region $0 \leqslant \eta \leqslant 1$, which simplifies the numerical method used for solution. This technique has previously been applied by e.g. Bonnecaze *et al.* (1993) to solve the shallow-water equations for a particle-driven gravity current in a horizontal channel, and by Bonnecaze *et al.* (1995) for axisymmetric particle-driven gravity currents. The implementation described here has previously been used by Ross, Tompkins & Parker (2004) to study cold pool evolution.

The SHARP scheme (see Leonard 1988) is used for the time-stepping of the equations. This incorporates flux-limiting terms to prevent the growth of spurious oscillations in the scheme. The integration scheme differs from the numerical scheme of Bonnecaze *et al.* (1993), who used a two-step Lax–Wendroff method. The numerical solutions of the shallow water equations on a cone show a hydraulic jump forming at the back of the current and propagating towards the head. Such hydraulic jumps occur for axisymmetric currents, even in the absence of a slope. A small amount of artificial viscosity is added in addition to the flux-limiting terms to smooth these shocks out and prevent numerical instability (see e.g. Bonnecaze *et al.* 1993). This additional viscosity term is only important where the gradients of velocity are large (i.e. near a shock) and it does not affect the solution away from these regions.

Numerical solutions for the height profile of the gravity current are shown in figure 1 for various times. Results are given both with and without entrainment and drag. It can be seen that in the absence of entrainment a shock rapidly forms at the rear of the head with the layer behind becoming extremely thin. As suggested in § 2.2, the majority of the fluid is found in the head of the current and the top of the head is nearly horizontal. The inclusion of entrainment leads to a gravity current in which the distinction between head and tail is less clear. The depth of the fluid remains non-zero behind the head, only tending to zero at the origin. The current also propagates more slowly. Figure 1(*c*) shows a current with both entrainment and bottom drag. The entrainment is reduced in this case compared to (figure 1*b*) so the overall propagation speed remains similar. Since the current is partly being retarded due to bottom drag rather than entrainment, the height of the current is less than in figure 1(*b*) and consequently the effective gravity is greater. The qualitative shape of the current is still set by the entrainment, with no clear divide between the head and tail of the current.

A more detailed comparison of the numeric solutions to the long-time asymptotic solutions is given in figures 2 and 3. For a slope of 5°, numerical solutions without entrainment tend towards the long-time behaviour predicted in § 2.2 (figure 2*b*). Convergence is very slow because it requires large values of r_f for the expansion parameter $r_f^{-1/4}$ to become small. The results are shown for a non-dimensional time of 15, by which stage the numerical and asymptotic profiles are very similar, although not identical. Agreement between them improves with time. Figure 2(*b*) shows that

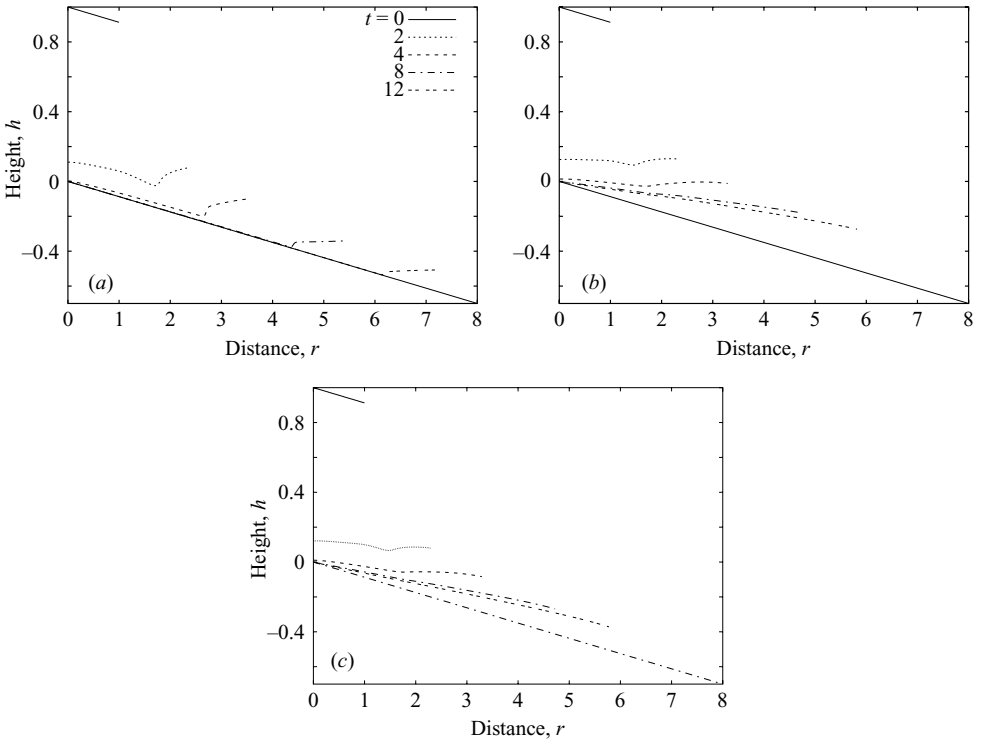

FIGURE 1. Profiles of a gravity current on a cone of slope 5.0° from the shallow-water model at a series of different times, t, after release. Results are shown in (a) for the solution without entrainment or drag, (b) for a solution with just entrainment ($\alpha = 0.1$, $C_d = 0.0$) and (c) for a solution with entrainment and drag ($\alpha = 0.05$, $C_d = 0.05$).

the asymptotic solution correctly predicts the shape of the current on the slope, but not the exact position because of the differences between the asymptotic expansion and the numerical solutions at early times. From figure 3(b) this offset in the position can be observed at all times, although it is relatively less significant for longer times. To predict the front position correctly in this case a constant offset may be applied to the time. An alternative is to use $r_f(t)$ as the independent variable rather than t, since the expansion is written in terms of r_f. In the absence of a slope (see figure 2a), the asymptotic solution is less useful. The numerical solution shows the formation of a hydraulic jump at the rear of the head which leads to a deeper (and hence faster) head with a shallower tail. The asymptotic solution is assumed continuous and so does not capture this behaviour. The formation of a deep head and very shallow tail is in fact closer to the observed behaviour of gravity currents in the laboratory.

Numerical solutions with entrainment show that for a slope of 5°, where (2.10) is satisfied, the similarity solutions are in fact the long-time solution for a lock release gravity current on a cone (figure 2b). In this case, the agreement is much better than for the non-entraining case, both in terms of the shape of the current and the front position. When the slope is 0° the similarity solution has the correct form for the front position, but the coefficient is such that it significantly underpredicts the front speed (see figure 3a). In cases where (2.10) is not satisfied, for instance if $\theta = 0$, then the solution looks similar, but the difference in behaviour at the origin where the similarity solution has a singularity results in a different propagation speed and a

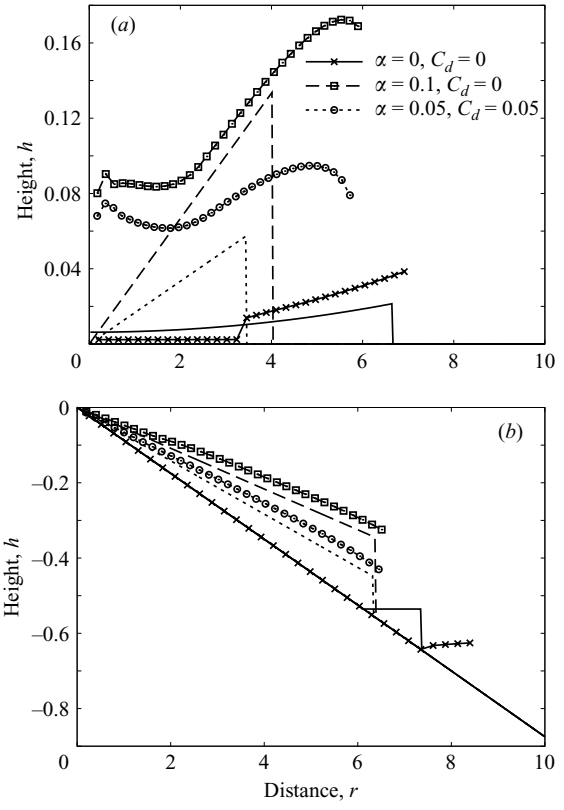

FIGURE 2. Profiles of an axisymmetric gravity current (*a*) on a flat surface and (*b*) on a cone of slope 5.0° from the shallow-water model, for various values of α and C_d, at time $t = 15$. Results are shown from both the numerical solutions and the asymptotic expressions. The points show the numerical solutions of the shallow-water equations and the lines show the similarity solution. The asymptotic solution in the absence of entrainment and drag, (A 11), is shown by the solid line. Solutions with entrainment and drag, (2.8*c*), are shown by dashed lines.

slightly different height and density profile, as seen in figure 2(*a*). In this case the front speed is greater than that predicted by the similarity solution and is in fact closer to the non-entraining similarity solution (figure 3*a*). This increased speed leads to increased entrainment and hence to a larger, but more dilute current.

3. A two-dimensional vorticity–streamfunction model

3.1. *Governing equations*

Assuming that the flow is incompressible, the Navier–Stokes equations can be written in the form

$$\rho \frac{\mathrm{D}\boldsymbol{u}}{\mathrm{D}t} = \rho \boldsymbol{g} + \nabla p + \rho \nabla \cdot (\nu \nabla \boldsymbol{u}), \tag{3.1}$$

$$\nabla \cdot \boldsymbol{u} = 0, \tag{3.2}$$

where $\boldsymbol{u}$ is the velocity of the flow, ρ is the density of the fluid, $\boldsymbol{g}$ is the acceleration due to gravity and ν is the kinematic viscosity. In what follows, ν is assumed to

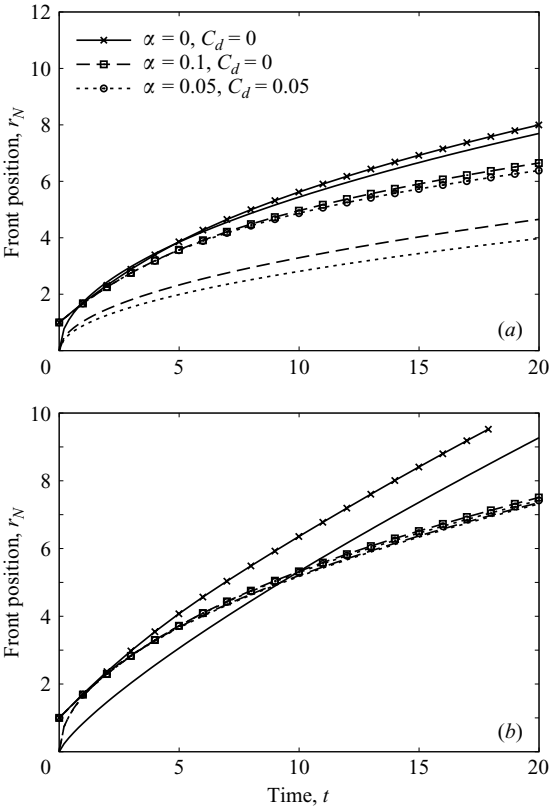

FIGURE 3. Front position against time for a gravity current on a cone of slope (*a*) 0° and (*b*) 5.0°. Results from the numerics (points) and the asymptotic solutions (lines) are shown for various values of α and C_d.

consist of a molecular diffusion term and a turbulent diffusion term. The latter is parameterized to represent the unresolved turbulent motions in the flow.

A gravity current is the result of fluids of two densities interacting. There may be a variety of causes for this density difference. It may be compositional, for example due to the release of a dense gas in the atmosphere, or due to the difference between saline and fresh water. It may also be due to differences in temperature, for example sea breezes or thunderstorm outflows. Whatever the cause of the density anomaly, we will assume a transport equation of the form

$$\frac{\mathrm{D}\chi}{\mathrm{D}t} = \nabla\cdot(\nu\nabla\chi), \tag{3.3}$$

for the scalar χ, be it salinity, fraction of dense gas or temperature anomaly. The density perturbation is assumed to be linearly related to the scalar χ. The effective diffusivity of the scalar, ν, is assumed to be equal to that of momentum as it is dominated by turbulent processes.

The Boussinesq approximation is made so that density variations are neglected, except in the buoyancy term where they appear combined with gravity. This simplifies the equations and is a reasonable approximation provided $\Delta\rho/\rho \ll 1$. For saline laboratory experiments this condition generally holds. It may not be true for the initial stages of a dense gas release, but once the cloud has diluted through entrainment it

becomes a better approximation. Making the Boussinesq approximation and taking account of the diffusion of the density variations gives the equation

$$\frac{\mathrm{D}g'}{\mathrm{D}t} = \nabla \cdot (\nu \nabla g'), \tag{3.4}$$

for the density perturbations where g' is again the effective gravity.

Taking the curl of (3.1) and making the Boussinesq approximation gives

$$\frac{\mathrm{D}\boldsymbol{\omega}}{\mathrm{D}t} = \nabla \times g' + \nabla \times \nabla \cdot (\nu \nabla \boldsymbol{u}), \tag{3.5}$$

where

$$\boldsymbol{\omega} = \nabla \times \boldsymbol{u} \tag{3.6}$$

is the vorticity of the flow. This is useful as it eliminates the pressure term in (3.1), so reducing the number of variables. Equations (3.4) and (3.5) describe the time evolution of the flow.

The turbulent eddy diffusivity is calculated assuming a Smagorinsky mixing length closure so that

$$\nu = \nu_{mol} + L^2 S, \tag{3.7}$$

where $L = C_s(\Delta x \Delta y)^{1/2}$ is the subgrid mixing length, $S^2 = \frac{1}{2} S_{ij} S_{ij}$, $S_{ij} = \partial u_i / \partial x_j + \partial u_j / \partial x_i$ is twice the rate-of-strain tensor and C_s is a constant, usually taken as 0.15.

It can be shown that for a two-dimensional, incompressible flow there always exists a streamfunction, $\psi(x, z)$, with

$$\boldsymbol{u} = \left(-\frac{\partial \psi}{\partial z}, 0, \frac{\partial \psi}{\partial x} \right) \tag{3.8}$$

in Cartesian coordinates. Similarly, for an axisymmetric flow a streamfunction, $\Psi(r, z)$, exists with

$$\boldsymbol{u} = \left(-\frac{1}{r}\frac{\partial \Psi}{\partial z}, 0, \frac{1}{r}\frac{\partial \Psi}{\partial r} \right) \tag{3.9}$$

in cylindrical polar coordinates. In both cases the vorticity is

$$\boldsymbol{\omega} = (0, \omega, 0). \tag{3.10}$$

Writing the equations of motion in terms of the streamfunction, ψ, ensures the incompressibility condition, $\nabla \cdot \boldsymbol{u} = 0$, is automatically satisfied, making the equations easier to solve. The velocity field can always be recovered by calculating the partial derivatives of ψ.

Substituting the streamfunction in (3.6) gives the Poisson problem

$$\nabla^2 \psi = -\omega \tag{3.11}$$

for the two-dimensional case. This is used to relate the vorticity ω and the streamfunction ψ in a two-dimensional channel flow. Given the vorticity together with suitable boundary conditions on ψ, (3.11) is inverted to obtain the streamfunction, from which the velocities can be easily calculated. For an axisymmetric flow, the relation between Ψ and ω is

$$\nabla^2 \Psi - \frac{2}{r}\frac{\partial \Psi}{\partial r} = -r\omega. \tag{3.12}$$

This formulation of the Navier–Stokes equations is frequently used because it separates the problem into two parts. First, the vorticity–streamfunction relationship

is inverted to obtain the streamfunction and hence the velocity field. Second, the velocity is used to advect the vorticity and effective gravity. This has one fewer variables than the initial problem, since there is no need to solve for the pressure field explicitly. Finding the pressure field is often the most difficult part of computational fluid dynamics problems.

Use of a high-resolution grid can capture the larger-scale eddies in the flow and thus resolve a large part of the mixing. The subgrid mixing is parameterized by the closure scheme. For gravity currents the large-scale mixing is principally a result of the formation of billows on the current interface induced by a shear instability. These billows are observed in the laboratory; however their growth is limited by further three-dimensional instabilities (see e.g. Simpson 1997). In a two-dimensional model this mode for breakdown of the billows is not available and so the billows tend to be larger than those observed in experiments.

Such vorticity–streamfunction models have successfully been used to study a variety of buoyancy-driven fluid flows such as particle-laden gravity currents (Huppert 1998), Rayleigh–Taylor instability (Dalziel 1998) and convection (Leppinen 1997).

3.2. *Boundary conditions*

In order to simulate flow in a channel or an axisymmetric flow we apply a free-slip boundary condition which assumes that the boundaries of the domain are solid with no flow through the wall. In particular, this means that the velocity tangential to the wall need not be zero, unlike a no-slip boundary condition. The boundary conditions on the vorticity and the effective gravity are that there is no flux through the solid boundaries.

3.3. *Method of solution*

Equations (3.4) and (3.5), together with (3.11) or (3.12) are solved numerically in a tilted rectangular domain with suitably applied initial and boundary conditions. The rectangular domain means that both the lower and upper boundaries are sloping. The solution consists of three stages. First, given ω, (3.11) or (3.12) is solved to find ψ (or Ψ). From ψ (or Ψ) the velocities u and w can be calculated. In the second stage, ω and g' are advected using these velocities. The third stage consists of the addition of the source terms for the baroclinic generation of vorticity.

The Poisson problem, (3.11) or (3.12), is solved using a full multigrid method similar to that described in Press *et al.* (1992). The multigrid method was found to provide an efficient and accurate method of solving this problem to the same order of accuracy as the discretization of the equations.

The advection scheme uses a staggered finite-volume grid. The vorticity ω and the effective gravity g' are stored at the centre of each grid square, and the streamfunction is stored at the corners of the square. Using central differencing, u is calculated on the sides of each square and w on the top and bottom of each square, as required to calculate the fluxes. This formulation ensures the conservation of buoyancy in the model.

The time-stepping of the equations of motion is achieved using the SHARP scheme (see Leonard 1988). The scheme is third order in space over most of the flow, but only first order in time. Where there are large density gradients in the flow the accuracy of the scheme is reduced to first order in space through the flux limiting terms. The flux limiting terms help to ensure the solution is accurate, but also remains stable near the front of the gravity current, where the density gradients are large.

Both the baroclinic term and the viscous term on the right-hand side of (3.5) can be written as a flux. These fluxes are incorporated with the advective flux terms in

the numerical model. This flux formulation ensures that buoyancy is conserved in the model. For a typical run the fractional change in total buoyancy over the course of simulation is less than 10^{-6}.

To ensure stability of the numerical scheme it is necessary that the CFL number

$$c = \frac{u\Delta t}{\Delta x} < 1, \tag{3.13}$$

where u is the fluid speed, Δt is the time step and Δx is the grid spacing. In practice the time step was chosen by setting $c = 0.25$ and choosing the minimum time step over all grid points so that

$$\Delta t = 0.25 \min_{i,j} \left(\frac{\Delta x}{u_{i,j}}, \frac{\Delta y}{v_{i,j}} \right). \tag{3.14}$$

3.4. *Model validation*

To validate the model several simulations were performed for some of the laboratory experiments presented in Huppert & Simpson (1980) for horizontal, axisymmetric gravity currents (experiments 1–6 in their table 2). The numerical results were compared with the published results from Huppert & Simpson (1980). Huppert & Simpson (1980) identify two distinct stages in the development of a gravity current. During the initial slumping phase the fractional depth of the current is relative deep compared to the depth of the tank. Empirically during this stage the Froude number, F, is a function of the fractional depth h_0/H with $F = \frac{1}{2}(h_f/H)^{-1/3}$, where h_f is the depth of the head and H is the depth of the tank. Once the fractional depth is less than 0.075 then the second stage is reached during which a constant Froude number of 1.19 was observed. Using an integral model the front position and height are calculated as a function of time, and from this the duration, t_s, of the slumping phase is estimated. Figure 4(a) shows the front position non-dimensionalized on the predicted front position as a function of time. This is analogous to figure 7 in Huppert & Simpson (1980). It can be seen that, as with the laboratory results of Huppert & Simpson (1980), the results from the different simulations collapse well and are in excellent agreement with the predicted front position. As a further test, figure 4(b) shows the front Froude number plotted against time. The numerical results show the two distinct stages of the flow. For $t/t_s < 1$ the gravity current is in the slumping phase, with the Froude number slowly increasing with time as the current slumps. For $t/t_s \gg 1$ the Froude number is approximately constant. There is a larger scatter in the Froude number results. There are two main reasons for this. First, there is an error associated with finite differencing the front position on a discrete grid to calculate the front speed. Second, there is some ambiguity in how to define and calculate $g'h$. Here we have taken the maximum value of $g'h$; however, there is some variation in this as billows evolve on the head of the current.

These numerical results are in good agreement with the findings of Huppert & Simpson (1980) suggesting that the numerical model is accurately representing the processes in a gravity current. There is, however, some suggestion from both the front position and Froude number that the slumping phase lasts slightly longer than predicted by Huppert & Simpson (1980). The predicted value is based on a simple integral model and so some discrepancy is perhaps not surprising. In fact, there is also some suggestion of this longer slumping phase in the experimental front position results plotted in figure 7 of Huppert & Simpson (1980).

Further comparisons were made with axisymmetric gravity current experiments conducted by Hallworth, Huppert & Ungarish (2001) (see figure 5) and Maxworthy

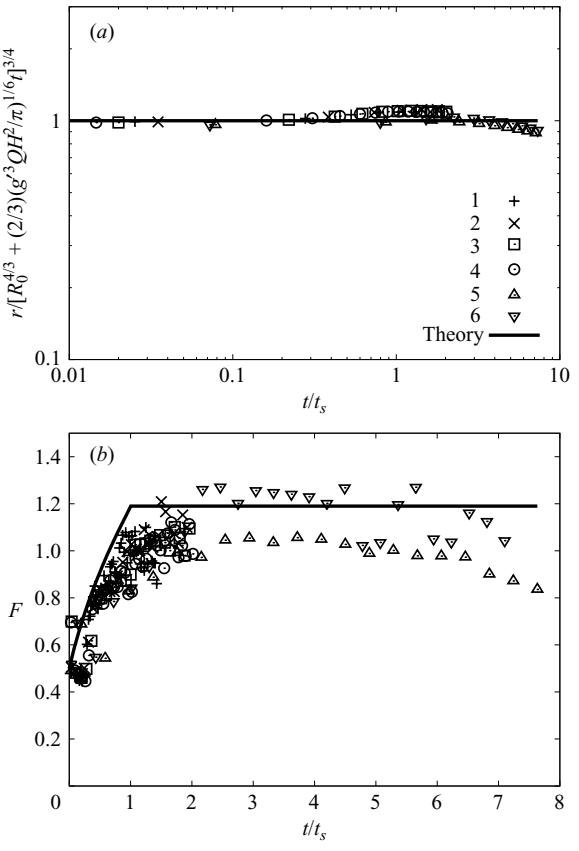

FIGURE 4. (*a*) Front position and (*b*) Froude number as a function of time for horizontal, axisymmetric gravity currents. Plotted are six numerical simulations based on experiments 1–6 from Huppert & Simpson (1980). Also shown are the front position and Froude number predicted by Huppert & Simpson using a simple integral model. Distance is non-dimensionalized with respect to the calculated front position during the slumping phase using the formula from Huppert & Simpson. Time is non-dimensionalized using the duration of the slumping phase, t_s.

et al. (2002) (not shown). These experiments included cases where the initial height of the release was less than the depth of water in the tank. Again, good agreement is observed between the experimentally determined front position and the results from the numerical simulations. For non-dimensional time up to about 10 the experimental results of Hallworth *et al.* (2001) and the numerical simulations are in excellent agreement. The simulations are a significant improvement over the integral model of Huppert & Simpson (1980) for example. There is a slight tendency to overpredict the propagation speed at later times. These features are also seen in the shallow-water model of Hallworth *et al.* (2001), which produces similar results to the present simulations in terms of predicting front position. The present simulations have the advantage of not requiring the empirically determined Froude number.

The overprediction in front speed is most likely to be due to the free-slip boundary condition used here. Its use neglects any drag caused by the lower boundary which would act to retard the gravity current. Two-dimensional direct numerical simulations of a gravity current in a flat channel by Härtel *et al.* (2000) suggest that using a free-slip boundary condition leads to an increase in front speed of about 20 %

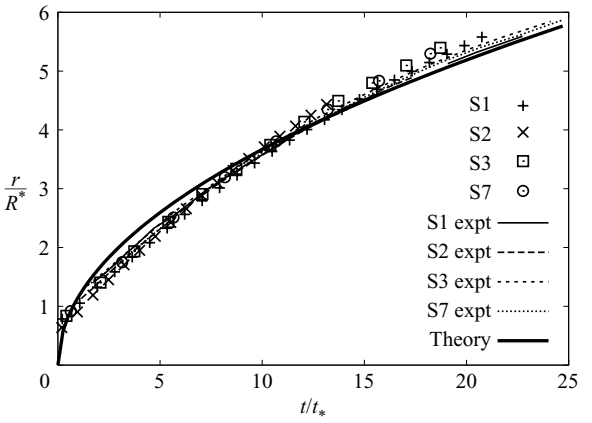

FIGURE 5. Front position as a function of time for horizontal, axisymmetric gravity currents. Plotted are four numerical simulations based on experiments S1, S2, S3 and S7 from Hallworth *et al.* (2001) (points). Also shown are the experimental measurements from these experiments (thin lines) and the values predicted by Huppert & Simpson using a simple integral model (thick line). Distance is non-dimensionalized with respect to $V^{1/3}$ and time with respect to $V^{1/6}/g_0'^{1/3}$.

compared to a no-slip boundary condition for moderate Reynolds numbers of about 700. As the Reynolds number increases the discrepancy between the speed of the free-slip and no-slip currents decreases, reducing to about 7 % for a Reynolds number of 3×10^4. The Reynolds number of these simulations is consistent with the experiments presented here. Comparison of two-dimensional and three-dimensional simulations by Härtel, Meiburg & Necker (2000) were in close agreement, suggesting that three-dimensional effects are not dominant in controlling the propagation of a gravity current, which supports the approach adopted here of using two-dimensional simulations for computational efficiency.

To further validate the model results were compared with the free-slip simulations of Härtel *et al.* (2000) for a lock release in a channel (not shown). In this case there was excellent agreement in the front position of the gravity current and also in the number, location and size of the billows on the interface between the dense and light fluid.

The results of these various test cases suggest that the numerical model described here can accurately simulate Boussinesq gravity currents. It is likely that the model will slightly overpredict the propagation speed of a current travelling along a solid surface as a result of the free-slip boundary condition employed. Previous work by Härtel *et al.* (2000) suggests that this effect will be reduced for higher-Reynolds-number flows.

4. Laboratory experiments

As is common in the study of gravity currents (see e.g. Simpson 1997), laboratory experiments were carried out using fresh water for the ambient fluid with salt added to create a density difference. A sector tank tilted at an angle was used for the experiments, rather than having a release on a cone. This has the advantage of taking up much less space so a longer slope can be used. It also enables the flow to be viewed from the side, allowing easier and more accurate comparison with the numerical code. Provided the sector is reasonably wide, it can be expected that

Expt	Slope (deg.)	Initial length r_0 (m)	Initial height h_0 (m)	Fractional depth	g'_0 (m s^{-2})	$V = \pi r_0^2 h_0$ (m^3)	Reynolds number
1	0	0.60	0.30	1.0	0.15	0.339	2.25×10^4
2	0	0.60	0.213	0.71	0.15	0.241	1.35×10^4
3	0	0.60	0.147	0.49	0.15	0.166	7.71×10^3
4	0	0.60	0.069	0.23	0.15	0.078	2.48×10^3
5	2.15	0.60	0.223	1.0	0.15	0.252	1.44×10^4
6	2.15	0.60	0.158	0.71	0.15	0.179	8.63×10^3
7	2.15	0.60	0.100	0.45	0.15	0.113	4.35×10^3
8	2.15	0.60	0.040	0.18	0.15	0.045	1.10×10^3
9	5	0.60	0.175	1.0	0.15	0.198	1.00×10^4
10	5	0.60	0.126	0.72	0.15	0.142	6.12×10^3
11	5	0.60	0.085	0.46	0.15	0.091	3.13×10^3
12	5	0.60	0.044	0.25	0.15	0.049	1.25×10^3

TABLE 2. Details of the experiments conducted. The height and fractional depths are average values over the length of the lock. The initial Reynolds number is calculated as $\sqrt{(g'_0 h_0/2)}(h_0/2)/\nu$.

the presence of the sidewalls will not play a significant role in the flow. Previous experiments on horizontal axisymmetric gravity currents have been carried out in a sector tank (see e.g. Huppert & Simpson 1980) and have been found to agree with experiments using a cylindrical release on a flat surface. In the present experiments a lock gate was placed near the apex of the sector tank, perpendicular to the floor of the tank. The tank was filled with water and salt was dissolved in the end behind the lock. A small amount of dye (potassium permanganate) was also added with the salt to allow the visualization of the denser fluid. The lock gate was quickly raised to release the dense salty fluid into the lighter ambient.

Experiments were recorded using a Cohu 4912 monochrome CCD camera connected to a Panasonic S-VHS AG-7350 video recorder. The results were digitized using a Data Translation DT2862 frame grabber card and the DigImage software (Dalziel 1992). The digitized images were subsequently analysed using the DigiFlow image processing system (Dalziel 2004). As well as providing a visual indication of the motion of the dense fluid, the presence of the dye allows more quantitative measurements to be made. First the propagation and shape of the gravity current may be accurately measured from the digitized images using known reference points on the tank. Secondly the concentration of the dye may be calculated by measuring the absorption of light by the dye. Since salt and the dye mix and diffuse in the same way the concentration of the salt can be inferred. Potassium permanganate is used in preference to other dyes because of its linear optical absorption properties. The method has previously been applied to a variety of laboratory problems and is described in more detail in e.g. Cenedese & Dalziel (1998). Using this method it is possible to obtain instantaneous measurements of the width-integrated concentration of salt within the gravity current. The width of the sector tank at any given point is calculated using the distance from the apex (measured from the digitized images) and the known angle of the sector tank. Using these g' can be derived.

A series of experiments with different slopes and with different fractional depths for the initial release were carried out. Full details of the experiments conducted are given in table 2. Slopes of 0°, 2.15° and 5° were used. By part filling the tank, dissolving salt in the lock and then slowly adding more fresh water on top it was possible to

set up releases where the initial depth of the dense fluid was less than the depth of the ambient fluid. With this method the top of the release was always horizontal. The heights given in table 2 are values averaged over the length of the lock. The fractional depth of the release, that is the average depth of the initial saline layer in the lock compared to the total average depth of water in the lock, varied between about 0.2 and 1.0 as shown in table 2.

When the sector is tilted, the tank does not exactly reproduce the geometry of a cone as the bottom of the tank is flat rather than curved in the azimuthal direction. The width of the tank is also not quite correct. However, the error is small for small slope angles and a small sector angle. The sector tank used for the experiments described here was 235 cm long, 41 cm deep and had a sector angle of 9.5°. Both the sector angle and the angle of the slope ($\leqslant 5°$) are sufficiently small to make the experiments a good approximation to a conical geometry. One further difference is that the endwalls of the tank are tilted rather than vertical. The top of the layer of ambient fluid is a free surface and so remains horizontal.

The aspect ratio for all the releases was relatively low, ranging from 0.08 to 0.5. This was limited by the length and depth of the tank. Initial Reynolds numbers were calculated assuming an initial speed of $\sqrt{g_0' h_0/2}$ and a lengthscale of $h_0/2$, where h_0 is the initial depth of the release, and are shown in table 2. They range from 1.10×10^3 to 2.25×10^4, so in all experiments the fluid was at least initially turbulent. To test the reproducibility of the experiments, experiment 1 was repeated 5 times. The front position was highly reproducible; however there was significant variability in the structure of the billows behind the head. Experiment 1 was also repeated for different values of g' with $g' = 0.05, 0.5, 1.0\,\mathrm{m\,s^{-2}}$. The results (not shown) collapsed well using the non-dimensionalization given in table 1.

5. Comparison of results

The vorticity–streamfunction numerical model described in § 3 was used to simulate the laboratory experiments described in § 4. Results were compared with the shallow water models of § 2 and with the experimental data.

5.1. *Experimental results and comparison with theory*

The asymptotic shallow-water solution of § 2.3 is only valid for slopes greater than about 1.9° so these experiments cover the case of no slope (0°) where the solution is not valid, a slope (2.1°) which is close to the critical value and a slope (5°) well above the critical value, but still small enough that the shallow-water equations are a good approximation.

The non-dimensional front position of the gravity current against time is plotted in figure 6 for the various experiments. For a given slope, the data for various fractional depths collapse fairly well. The initial fractional depth of the release appears to make only a relatively small difference to the propagation speed of the current. A larger effect has been noted for the initial stages of lock-release gravity currents in a horizontal two-dimensional channel (see Huppert & Simpson 1980); however the radial geometry used here means that as the current spreads it decreases in height more rapidly than the two-dimensional case, reducing the effect of the fractional depth. The presence of the slope also acts to increase the depth of the ambient fluid as the current propagates downslope which reduces the fractional depth. Once the fractional depth becomes small, perhaps <0.1, the current is not significantly affected by the actual depth of fluid above it and the ambient fluid may be considered to be

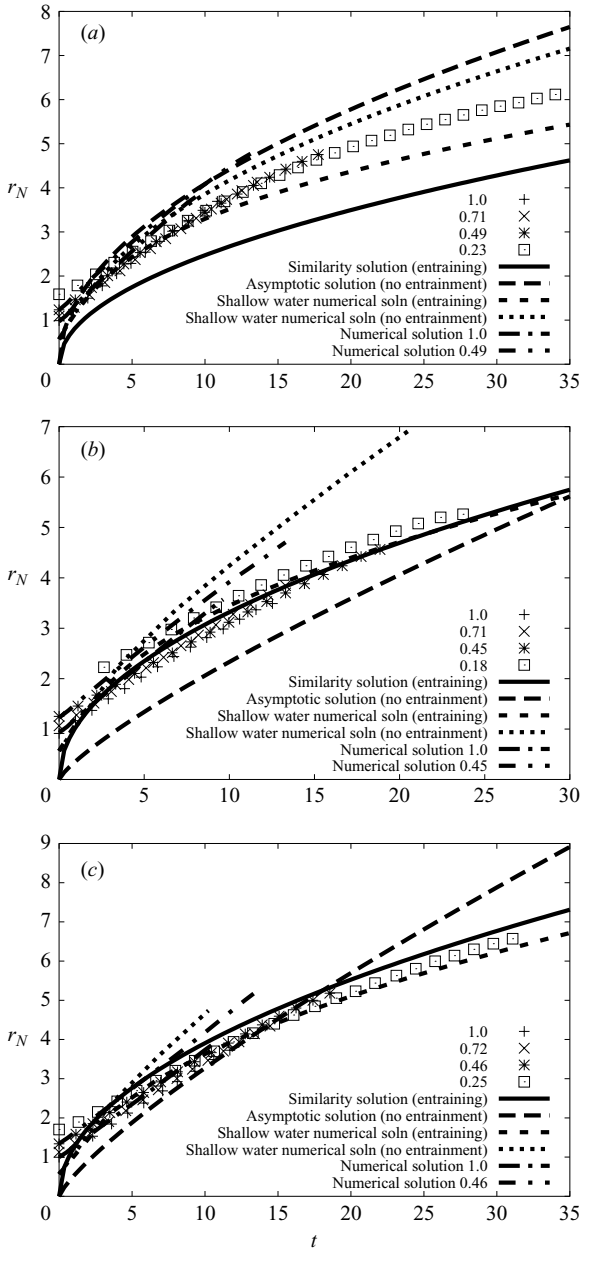

FIGURE 6. Front position against time for flow down a cone. Results from both the experiments (with different fraction depths indicated by the legend) and from the shallow water models are given for various slopes. Distance is non-dimensionalized with respect to V_0 and time with $V_0^{1/6}/g_0'^{1/2}$.

infinitely deep. This suggests that, except very close to the release point, the fractional depth is not significant in controlling the speed of the current for flow down a cone.

Figure 6 also shows the results of the shallow-water models given in § 2 and the numerical model of § 3. The shallow-water model without entrainment overpredicts the front position when compared to the experiments. This is in agreement with the

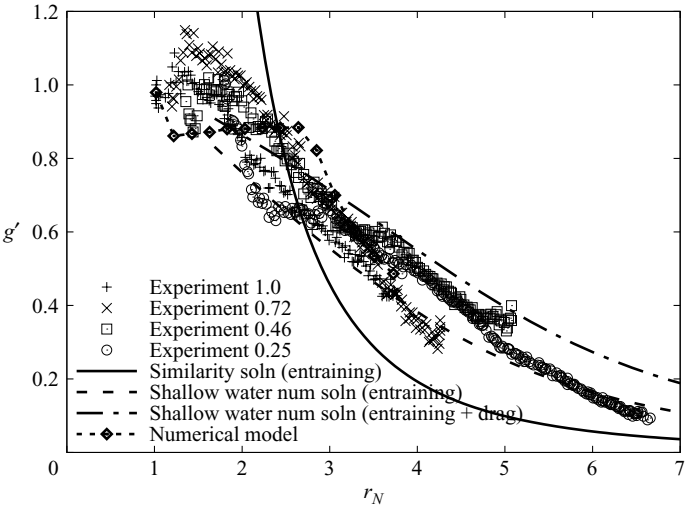

FIGURE 7. Effective gravity of the current front against front position for flow down a cone of 5° slope. Results are shown from the experiments (with different fraction depths), from the shallow water models and from the streamfunction–vorticity model (with a full depth release). The effective gravity is non-dimensionalized with respect to g_0' and distance with respect to $V_0^{1/3}$.

findings of other studies (e.g. Tickle 1996; Ross *et al.* 2002) of gravity currents on a slope. For the slope of 5°, the shallow-water model with entrainment gives much closer agreement with the experimental data. For lower slopes, where (2.10) is not satisfied, the entraining asymptotic solution underpredicts the front position when compared with experimental data. The numerical model is in good agreement with the experimental results over a range of slopes, although there is a slight tendency to overpredict the front position. This is consistent with the use of a free-slip boundary condition. For the Reynolds numbers of the experiments described here this error is expected to be less than 10 % based on the results of Härtel *et al.* (2000).

The numerical simulation assumes a rigid lid parallel to the bottom of the computational domain so the depth of the channel is constant, in contrast to the experiments where the free surface is horizontal and the depth of the channel varies. To take this into account, an average lock depth was used as the channel depth for the numerics to ensure that there was the same volume of fluid in the lock in each case. The experimental and numerical results agree well despite the differences in the geometry. As discussed above, the fractional depth is less important in an axisymmetric geometry than in a channel as the axisymmetric current becomes thinner much more rapidly.

Figure 7 shows the effective gravity of the head against the front position for a slope of 5°. The experimental data with different initial fractional depths collapse well, again showing the relative insensitivity of the flow to the initial fractional depth. From the data there appears to be a nearly linear decrease of g' in the head. This suggests that a significant amount of entrainment is occurring and this cannot be ignored in the modelling. In the absence of entrainment the shallow-water model assumes a constant value for g', and this is clearly not a good assumption. The entraining similarity solution for the shallow-water equations gives a more realistic decrease in g' with distance, although with a typical value of $\alpha = 0.1$ for the entrainment constant

and a slope of 5° it predicts that $g' \sim r_f^{-2.25}$ rather than decreasing linearly. Numerical solutions to the shallow-water equations show that in practice the solution has not quite reached the similarity solution in the regime covered by the experiments. These shallow-water numerical solutions are in much better agreement with the experimental data. Results are shown with an entrainment coefficient, $\alpha = 0.1$ and no drag and also with $\alpha = 0.05$, $C_d = 0.05$, both of which give very similar predictions for the front position in agreement with the experimental results. The dilution of the current is reduced with the reduction in entrainment, and so higher values of g' are predicted at the head. All the experimental data appear to lie somewhere between these two curves. This suggests that for this case entrainment is more important, although bottom drag still plays a role. Results are also shown for the streamfunction–vorticity model. Here the value of g' at the front is calculated from the model results by taking an average value over the head (defined as the region up to 90 mm (80 grid points) behind the front). The threshold for determining the edge of the current is taken as $0.05\, g'_{max}$, where g'_{max} is the maximum value of g' in the current at that time. The values from the numerical model for the effective gravity at the front of the current are also in close agreement with the experimental values. Since this is an average value of g' over the head, similar results are obtained with and without the inclusion of the turbulence closure term in the numerical model. This suggests that the mixing within the head of the current is predominantly a result of the large-scale billows, rather than of very small-scale turbulent processes. The small-scale turbulent processes tend just to smooth out the fine-scale structure, at least in the model results. The scatter in the values of g' measured at the front of the head in the numerical simulations is principally a result of the formation, growth and subsequent decay of shear-induced billows on the interface between the dense fluid in the gravity current and the lighter ambient fluid. This scatter is minimized by taking the value of g' averaged over the head. Both experimental and numerical results exhibit slightly more complicated behaviour than the shallow water model, with values of g' initially changing very slowly as the current slumps. This is slightly more pronounced in the numerical model and corresponds with previous research on horizontally propagating gravity currents, which suggests that entrainment is not important during the slumping phase (Hallworth *et al.* 1996).

To test the constant Froude number condition (2.4) used in the shallow water model, the front Froude number from the numerics was calculated. The value of $g'h$ used in this calculation was the maximum depth-integrated value of g' in the head. The results are shown in figure 8. It can be seen that initially there is a rapid increase in the Froude number from around 0.6 to about 1.2 as the current develops. After this the Froude number remains relatively constant at about 1.2. The large scatter in the results is due to the evolution of the billows on the head of the current, making it difficult to unambiguously measure the Froude number. The results indicate that the constant Froude number assumption made in the shallow-water model is valid, at least once the current has developed. The value of 1.2 is in excellent agreement with the value of 1.19 assumed for the shallow-water model based on experiments in a flat channel by Huppert & Simpson (1980). For longer times (distances greater than about 3.5) there is some indication that the Froude number increases slightly for gravity currents where there is a slope. In these cases the current is very thin though, and so this may be a result of the current not being adequately resolved. This particular feature is also dependent to some extent on the method used to calculate $g'h$. This may be worthy of further experimental investigation. We note that these values for the Froude number cannot be directly compared with studies by Shin,

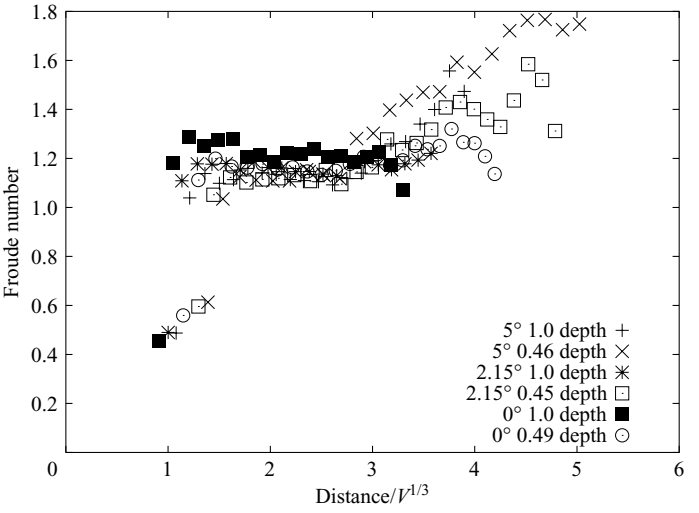

FIGURE 8. Froude number plotted against front position for a gravity current flowing down a cone. Results calculated from the numerics are plotted for various slopes and fractional depths of release. The front position is non-dimensionalized with respect to $V_0^{1/3}$.

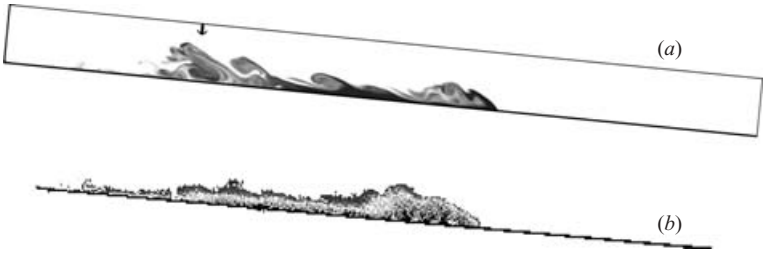

FIGURE 9. Density of a gravity current flowing down and up a sloping cone with a slope of 5.5°: (*a*) numerics and (*b*) experiments. The images are taken at a non-dimensional time of 6.0 corresponding to a front position of 2.5 lock lengths. The position of the lock is marked with an arrow.

Dalziel & Linden (2004) of the initial 'lock exchange' problem in a channel which use a Froude number based on the total channel depth because of the difference in fractional depth.

Figure 9 shows images from an experiment and the corresponding density field from the numerics. Both images were taken 12 s after the release, corresponding to a non-dimensional time of 6.0. In addition to predicting the front position of the gravity current accurately, the numerics provide a good description of the shape and size of the current. The head of a current flowing down a cone is seen to be well defined and contain most of the dense fluid. Note that the total amount of dense fluid is proportional to rg' since this is an axisymmetric flow. Behind the head is a thin layer of slightly less dense fluid. This layer does not stretch all the way back to the origin. The differences in this thin layer can be attributed to the lower boundary condition and the lack of a three-dimensional mechanism to dissipate the billows. In the numerical model results the billows appear deeper than the corresponding experimental results, although they do not contain significantly more dense fluid. It

appears that the details of the flow in this thin layer do not have a significant impact on the propagation and development of the head, which is our primary interest.

5.2. *Sensitivity to resolution and viscosity*

Calculations were carried out to test the sensitivity of the numerical model to the grid resolution. Standard simulations of the experiments described in § 5.1 were carried out on a 1024×128 grid with an equivalent experimental grid spacing of about 2.3 mm. A simulation for the 5° slope was also carried out at twice the resolution so the grid spacing was approximately 1.1 mm. The increased resolution increased the observed fine-scale structure in the billows, but made less than 1 % difference to the propagation speed of the current and less than 2 % difference to the depth of the head. The envelope of the gravity current behind the head was quantitatively altered by the change of resolution as a result of the Kelvin–Helmholtz instability; however the qualitative position and size of the billows was similar in both simulations and mean profiles of height (not shown) were in good agreement. During the course of these two simulations there is also little difference in the averaged value of g' calculated at the front of the gravity current. From this we conclude that the resolution is sufficient to resolve the important dynamic processes included in the model.

A similar sensitivity test was carried out on the role of the turbulent viscosity in the results. The standard simulation described above was repeated with $\nu = 0$ (both turbulent and molecular viscosities set to zero). There were qualitative differences between the two simulations. In particular much more fine-scale structure was observed in the inviscid simulation, with billows containing thin filaments of dense and ambient fluid. With the turbulence model turned on these tended to be mixed together to give more gradual changes in density. Despite these differences in the detailed structure, the bulk properties, such as the front position, were virtually unchanged between the two simulations, at least during the slumping phase of the flow. At later times when the current is much slower the viscosity plays an increasingly important role in controlling the gravity current. In such cases a no-slip boundary current should be used in place of the free-slip condition used in this study.

6. Conclusions

The presence of a small conical slope has been shown to make a significant difference to the propagation and development of an axisymmetric gravity current both theoretically and experimentally.

A solution of the shallow-water equations analogous to those of Webber *et al.* (1993) for a sloping channel cannot be found in this situation because the reduction in height due to the radial spreading prevents a constant-speed solution from being reached. Numerical solutions of the non-entraining shallow-water equations overpredict the front speed, as observed for other gravity currents in sloping channels or on a sloping plane. Inclusion of entrainment and drag within the shallow-water model leads to much better agreement on the front position of the gravity current and on the density within the head. It also allows a similarity solution to be found. The structure of the current for these cases is quite different. Without entrainment the current occupies a region of relatively constant length behind the head, while the asymptotic solution with entrainment predicts the current extending back to the origin for all time.

The behaviour predicted by the shallow-water model with entrainment is in much better agreement with laboratory experiments than the version without entrainment. Predictions of the front position, current shape and the density of the head are all

significantly improved. This highlights the important role of entrainment and drag in the flow of gravity currents on slopes in limiting the acceleration due to the slope. The important parameter in controlling the propagation speed is the ratio of the entrainment coefficient to the tangent of the slope, $\alpha/\tan\theta$. The relative importance of entrainment and drag is controlled by the ratio α/C_d.

The numerical streamfunction–vorticity model gives a simple and accurate way of modelling this type of flow with the added advantage of providing a more detailed picture of the structure of the current than the simpler shallow-water model. For flow down a cone the head is similar to the head of a current in a sloping channel, with the fluid in the head only being slowly mixed with the ambient fluid. The axisymmetric geometry means that the height of the current reduces rapidly as the flow expands radially.

The model captures many of the features observed in laboratory experiments. In particular, the model demonstrates the characteristic shear-induced billows on the gravity current head, which are ignored in many simple theories, but may be important for the mixing of the fluids. Being two-dimensional, the model cannot exhibit the lobe and cleft structure of the current front observed in experiments, nor does it capture the three-dimensional breakdown of the billows. The use of a free-slip boundary condition does result in a slight overprediction of the propagation speed of the current; however this error becomes less significant for high Reynolds numbers.

One further advantage of the numerical model is that it includes the ambient fluid as well as the gravity current. The flow in the ambient fluid has been shown to have a significant effect, particularly where the current occupies a significant fraction of the channel depth. The numerical model can accurately simulate such situations, unlike the one-layer shallow-water models. The numerical model has been demonstrated to be a useful tool in investigating a variety of gravity current flows. In addition to performing at least as well as existing simple models for predicting the speed and height of a current, it can also give a more detailed insight into some aspects of the complicated structure present in a range of other problems.

Flows directed towards the origin were not considered in this work, although they can be modelled using the vorticity–streamfunction code, provided that care is taken at the origin. Such a flow could result from a release of dense gas near the mouth of a valley. Such flows are however less amenable to the shallow-water and asymptotic modelling techniques described here.

Here we have looked at the specific problem of a gravity current flowing down a cone through the use of various modelling techniques and through laboratory experiments. In addition to the obvious benefit of being able to model such flows on cones, this work has some important wider applications. The presence of a slope appears to alter the dynamics of a gravity current significantly. In particular, entrainment and drag appear to play an important role in limiting the acceleration of the current. We would expect them to play a similar role over more complicated terrain. Although entrainment is clearly important to this, and a range of other problems related to gravity currents, there are still gaps in our understanding of the precise mechanisms by which gravity currents entrain ambient fluid and possibly detrain dense fluid. Further detailed laboratory experiments are still needed to shed some light on this.

A. N. R. was supported in this work while at DAMTP by an EPSRC CASE award in conjunction with the UK Health and Safety Executive. The authors would like to thank Nicolas Dispot, a visitor to DAMTP, for carrying out some of the experiments

described here. We would also like to thank Mark Hallworth for providing the experimental data shown in figure 5.

Appendix A. An asymptotic expansion without entrainment or drag

As discussed in § 2.2, the leading order term in the solution of (2.5)–(2.6) is given by $u = F\ (\tan\theta/\pi)^{1/4} r_f^{-1/4}$ and $h = (l - r_f + r)\tan\theta$ for $r_f - l \leqslant r \leqslant r_f$ where $l = (r_f \pi \tan\theta)^{-1/2}$. The neglected terms are $O(r_f^{-3/2})$ smaller. This suggests a change of variables with $y = (r - r_f)/l$ so y is $O(1)$ in the current and $y = 0$ at the head of the current. Consideration of the first neglected terms suggests an expansion of the form

$$u = F\left(\frac{\tan\theta}{\pi}\right)^{1/4} r_f^{-1/4}\left(1 + u_1(y)(\pi\tan\theta)^{-1/2} r_f^{-3/2}\right), \tag{A 1}$$

$$h = \left(\frac{\tan\theta}{\pi}\right)^{1/2} r_f^{-1/2}\left(1 + y + h_1(y)(\pi\tan\theta)^{-1/2} r_f^{-3/2}\right), \tag{A 2}$$

where u_1 and h_1 are order 1 functions. The boundary condition that $\dot{r}_f = u(r = r_f)$ yields

$$\dot{r}_f = F\left(\frac{\tan\theta}{\pi}\right)^{1/4} r_f^{-1/4}\left(1 + u_1(0)(\pi\tan\theta)^{-1/2} r_f^{-3/2}\right). \tag{A 3}$$

Substituting these expansions into (2.5) and equating terms of $O(r_f^{-3/2})$ yields the differential equation

$$(1 + y)\frac{\mathrm{d}u_1}{\mathrm{d}y} + u_1(y) = u_1(0) - (\tfrac{1}{2} + y), \tag{A 4}$$

which has the solution

$$u_1(y) = u_1(0) - \tfrac{1}{2}y. \tag{A 5}$$

Further substitution of this solution into (2.6) gives the differential equation

$$\frac{\mathrm{d}h_1}{\mathrm{d}y} = \frac{F^2}{4}. \tag{A 6}$$

Integrating and the applying the Froude number condition at the front gives

$$h_1(y) = \tfrac{1}{4}F^2 y + 2u_1(0). \tag{A 7}$$

The global conservation-of-volume equation in terms of y is

$$2\int_{-1+l_1 r_f^{-3/2}}^{0} \left(1 + y r_f^{-3/2}(\pi\tan\theta)^{-1/2}\right) \times \left[1 + y + r_f^{-3/2}(\pi\tan\theta)^{-1/2}\left(\tfrac{1}{4}F^2 y + 2u_1(0)\right)\right]\mathrm{d}y = 1. \tag{A 8}$$

It turns out that the precise form of l_1 is not important at $O(r_f^{-3/2})$. Setting the sum of the $O(r_f^{-3/2})$ terms to zero gives

$$u_1(0) = \tfrac{1}{8}\left(F^2 + \tfrac{2}{3}\right). \tag{A 9}$$

This give the expressions

$$u = F\, r_f^{-1/4}\left(\frac{\tan\theta}{\pi}\right)^{1/4}\left[1 + \left(\tfrac{1}{8}\left(F^2 + \tfrac{2}{3}\right) - \tfrac{1}{2}y\right)(\pi\tan\theta)^{-1/2} r_f^{-3/2}\right], \tag{A 10}$$

and

$$h = r_f^{-1/2}\left(\frac{\tan\theta}{\pi}\right)^{1/2}\left[1 + y + \tfrac{1}{4}\left(F^2(1+y) + \tfrac{2}{3}\right)(\pi\tan\theta)^{-1/2} r_f^{-3/2}\right], \tag{A 11}$$

where the transformed variable $y = (r - r_f)/l$ is order 1 and $y = 0$ at the head of the current.

The effect of including the second term in the asymptotic expansion is to deepen the front height, and hence increase the front speed, for a given front position. The cumulative effect of this is to increase the propagation speed of the current with time. Comparison of the asymptotic solution with the numerical solution for a 5° slope (not shown) demonstrates that the expression for the height of the current as a function of the front position is in excellent agreement with the numerical solution for front positions more than about three times the initial release radius. The agreement with the speed of the current is less good, requiring something like six times the distance before the condition is met. At this distance the correction from the second term in the asymptotic expansion is small and does not significantly alter the predicted velocity profile of the current.

Unfortunately integration of (A 3) does not lead to a simple expression for r_f in terms of t. Provided the singularity at $r_f = 0$ is avoided, however, the differential equation can easily be numerically integrated. Note that the relative inaccuracy of the asymptotic solution near the origin will lead to an offset in the predicted front position as a function of time.

Appendix B. A similarity solution for the sloping channel

For a gravity current in a sloping channel the shallow-water equations (including entrainment and drag) are

$$\frac{\partial h}{\partial t} + \frac{\partial uh}{\partial x} = \alpha|u|, \tag{B 1}$$

$$\frac{\partial uh}{\partial t} + \frac{\partial}{\partial x}\left(u^2 h\right) + \frac{\partial}{\partial x}\left(\frac{1}{2}g'h^2\right) - g'h\tan\theta = -C_d u^2, \tag{B 2}$$

and

$$\frac{\partial g'h}{\partial t} + \frac{\partial ug'h}{\partial x} = 0. \tag{B 3}$$

Letting $y = x/x_f$ and writing

$$u = xt^{-1}U(y), \tag{B 4}$$

$$h = xH(y), \tag{B 5}$$

$$g' = xt^{-2}G(y), \tag{B 6}$$

gives the similarity solution

$$x_f = B^{1/3}t^{2/3}\left[\frac{4}{3A}\left(-\frac{1}{3}\left(1 + \frac{4C_d}{3\alpha}\right) + \left(\frac{A}{3F^2} + 1 + \frac{4C_d}{3\alpha}\right)\frac{1}{3 - A}\right)\right]^{-1/3}, \tag{B 7}$$

$$U(y) = \tfrac{2}{3}, \tag{B 8}$$

$$H(y) = 1/(2\alpha), \tag{B 9}$$

$$G(y) = \frac{8}{3\alpha}A^{-1}\left(-\left(1 + \frac{4C_d}{3\alpha}\right) + \left(\frac{A}{3F^2} + 1 + \frac{4C_d}{3\alpha}\right)y^{-A}\right), \tag{B 10}$$

where

$$A = 3 - \frac{4\tan\theta}{\alpha}. \tag{B 11}$$

As in the axisymmetric case, the requirement that g' remains finite as $x \to 0$ gives a condition on the slope that

$$\tan\theta > \alpha/2, \tag{B 12}$$

in order for this solution to be valid. Note that this solution can be contrasted with the non-entraining shallow-water model of Webber *et al.* (1993) which gives a current with a constant shape and front speed.

REFERENCES

Beghin, P., Hopfinger, E. J. & Britter, R. E. 1981 Gravitational convection from instantaneous sources on inclined planes. *J. Fluid Mech.* **107**, 407–422.

Bonnecaze, R. T., Hallworth, M. A., Huppert, H. E. & Lister, J. R. 1995 Axisymmetric particle driven gravity currents. *J. Fluid Mech.* **294**, 93–121.

Bonnecaze, R. T., Huppert, H. E. & Lister, J. R. 1993 Particle-driven gravity currents. *J. Fluid Mech.* **250**, 339–369.

Britter, R. E. & Linden, P. F. 1980 The motion of the front of a gravity current travelling down an incline. *J. Fluid Mech.* **99**, 531–543.

Cenedese, C. & Dalziel, S. B. 1998 Concentration and depth fields determined by the light transmitted through a dyed solution. In *Proc. 8th Intl Symp. on Flow Visualization, Sorrento, Italy, 1–4 September 1998* (ed. Carlomagno & Grant).

Cheong, H. B. & Han, Y. H. 1997 Numerical study of two-dimensional gravity currents on a slope. *J. Oceanogr.* **53**, 179–192. Oceanographic Society of Japan.

Dalziel, S. B. 1992 *Digimage: System Overview*. Cambridge Environmental Research Consultants, Ltd.

Dalziel, S. B. 1998 Application of a general purpose CFD package to Rayleigh–Taylor instability. In *Proc. 6th Intl Workshop on Physics of Compressible Turbulent Mixing* (ed. G. Jourdan & L. Houas), pp. 139–144. Imprimerie Caractare, Marseille, France.

Dalziel, S. B. 2004 *Digiflow User Guide*. http://www.damtp.cam.ac.uk/lab/digiflow/.

Ellison, T. H. & Turner, J. S. 1959 Turbulent entrainment in stratified flow. *J. Fluid Mech.* **6**, 423–448.

Grundy, R. E. & Rottman, J. W. 1985 The approach to self-similarity of the solutions of the shallow-water equations representing gravity current releases. *J. Fluid Mech.* **156**, 39–53.

Hallworth, M. A., Huppert, H. E., Phillips, J. C. & Sparks, S. J. 1996 Entrainment into two dimensional and axisymmetric turbulent gravity currents. *J. Fluid Mech.* **308**, 289–311.

Hallworth, M. A., Huppert, H. E. & Ungarish, M. 2001 Axisymmetric gravity currents in a rotating system: experimental and numerical investigations. *J. Fluid Mech.* **447**, 1–29.

Härtel, C., Meiburg, E. & Necker, F. 2000 Analysis and direct numerical simulation of the flow at a gravity-current head. Part 1. Flow topology and front speed for slip and no-slip boundaries. *J. Fluid Mech.* **418**, 189–212.

Huppert, H. E. 1998 Quantitative modelling of granular suspension flows. *Phil. Trans. R. Soc. Lond.* A **356**, 2471–2496.

Huppert, H. E. & Simpson, J. E. 1980 The slumping of gravity currents. *J. Fluid Mech.* **99**, 785–799.

Leonard, B. P. 1988 Simple high accuracy resolution program for convective modelling of discontinuities. *Intl J. Numer. Methods Fluids* **8**, 1291–1318.

Leppinen, D. M. 1997 Aspects of convection. PhD thesis, DAMTP, University of Cambridge.

Maxworthy, T., Leilich, J., Simpson, J. E. & Meiburg, E. H. 2002 The propagation of a gravity current into a linearly stratified fluid. *J. Fluid Mech.* **453**, 371–394.

Montgomery, P. J. & Moodie, T. B. 1999 Two-layer gravity currents with topography. *Stud. Appl. Maths* **102**, 221–266.

Morton, B. R., Taylor, G. I. & Turner, J. S. 1956 Turbulent gravitational convection from maintained and instantaneous sources. *Proc. R. Soc. Lond.* A **234**, 1–23.

Press, W. H., Teukolsky, S. A., Vetterling, W. T. & Flannery, B. P. 1992 *Numerical Recipes in C*, 2nd edn. Cambridge University Press.

Ross, A. N., Linden, P. F. & Dalziel, S. B. 2002 A study of three-dimensional gravity currents on a uniform slope. *J. Fluid Mech.* **453**, 239–261.

Ross, A. N., Tompkins, A. M. & Parker, D. J. 2004 Simple models of the role of surface fluxes in convective cold pool evolution. *J. Atmos. Sci.* **61**, 1582–1595.

Shin, J. O., Dalziel, S. B. & Linden, P. F. 2004 Gravity current produced by lock exchange. *J. Fluid Mech.* **521**, 1–34.

Simpson, J. E. 1997 *Gravity Currents in the Environment and the Laboratory*, 2nd edn. Cambridge University Press.

Tickle, G. A. 1996 A model of the motion and dilution of a heavy gas cloud released on a uniform slope in calm conditions. *J. Haz. Mat.* **49**, 29–47.

Ungarish, M. & Zemach, T. 2005 On the slumping of high Reynolds number gravity currents in two-dimensional and axisymmetric configurations. *Eur. J. Mech.* B – *Fluids* **24**, 71–90.

Webber, D. M., Jones, S. J. & Martin, D. 1993 A model of the motion of a heavy gas cloud released on a uniform slope. *J. Haz. Mat.* **33**, 101–122.